Coincidence electron spectroscopy of W(100) in the threshold-energy region

O. M. Artamonov,* S. N. Samarin,* and J. Kirschner
Max-Planck-Institut für Mikrostrukturphysik, Halle, Germany
(Received 28 April 1994)

The simultaneous emission of two electrons from W(100) after excitation by a normally incident primary electron is studied as a function of the primary electron energy (10–22 eV relative to the Fermi level) and emission angle. We found that the coincidence rate as a function of the primary electron energy had a low-intensity tail in the region below 18 eV with an energy threshold at 11.5–12 eV. The most probable angle between two scattered electrons was found to be about 80° at 20.6-eV primary electron energy. The maximum sum energy of correlated electrons is found to agree with the energy conservation law limit. Experimental results are in fair agreement with calculations based on a two-parabolic-band approximation.

INTRODUCTION

The basic idea of a two-electron coincidence experiment of the type one electron in–two electrons out $(e,2e)$ is to measure the energy and momentum of a target electron participating in the collision event, when the energy and momentum of the incident electron are known. This yields information about the scattering process and the initial state of the target electron.

Transmission electron $(e,2e)$ experiments at high energy were carried out with thin films for studying the electronic structure of solids.[1] The spectral momentum density of carbon, graphite, aluminum, and aluminum oxide was measured[2] and experimental results for graphite have been compared with first-principles calculations.[3] A fair agreement between the theory and experiment was shown. Two-electron coincidence spectroscopy was also used to study the generation mechanisms of secondary and Auger electrons,[4] as well as for the determination of the production pathways of secondary electrons.[5]

In order to study the electronic structure of the solid surface and low-energy electron scattering dynamics by means of $(e,2e)$ spectroscopy, we used an electron coincidence spectrometer in the back-reflection geometry.[6] In our previous papers we have shown that true coincidence events can be observed in the reflection geometry experiment with low primary-electron energy.[6,7] The threshold energy of the appearance of correlated electrons was found to be approximately four times the work function of the sample surface.[6] When the work function is changed by means of adsorbate deposition, the energy threshold follows these changes.

In this paper we present further experimental results obtained with an improved $(e,2e)$ spectrometer yielding higher sensitivity. This was achieved by using multichannel plates (MCP's) as electron detectors with apertures larger than those of the channeltrons used in Ref. 6. We measure the coincidence-event (CE) number as a function of incident electron energy and of applied retarding potential, as well as the angular distribution of correlated pairs. The coincidence technique allows us to select only those time-correlated pairs of emitted electrons which are produced by one primary electron. The detected correlated pairs, however, can in principle be created both in single electron-electron scattering events and in a multiscattering process. From now on we shall refer to the detection of a correlated pair produced in a single scattering event as the true coincidence event (TCE) and to that of a correlated pair created in a multiscattering process as a secondary-electron coincidence event (SECE). A simple kinematic model of the creation of correlated electron pairs is formulated and the calculations are compared with experimental results. Fair agreement is found.

EXPERIMENTAL SETUP

The coincidence spectrometer used in our experiment is schematically shown in Fig. 1. An electron gun supplies 5–100-eV electrons, the electron beam diameter being not more than 3 mm. We used two MCP-based detectors which had two parallel grids each for the energy analysis of electrons leaving the sample. The detectors and the electron gun lie in the same plane passing through the sample surface normal. The angular position of the detectors and of the gun could be varied from 30° to 80° relative to the surface normal. The MCP's used in the experiment had an effective area of about 27 mm in diameter. To increase the low-energy-electron detection efficiency, an accelerating potential of about 300–400 V was applied between the MCP entrance and the nearest (second) grid. The distance between the sample and the first grid (i.e., the path length traveled by scattered electrons in the field-free region) was about 90 mm. In this geometry, the solid angle inside which electrons were gathered was ~ 0.07 sr, which allowed us to increase substantially the experimental accuracy compared to that in Ref. 6, where we used two channeltrons as detectors. A tungsten single crystal, 4×8 mm^2 in size, was mounted on two tungsten rods and could be heated up to 2000 °C by resistive heating for cleaning. The construction of the holder allowed us to turn the crystal in the azimuthal plane. The surface purity and its perfection were monitored by measuring relative intensities of diffraction maxima. The intensities of the following diffraction beams were measured: (01) from the tungsten surface, $(\frac{1}{2}\frac{1}{2})$

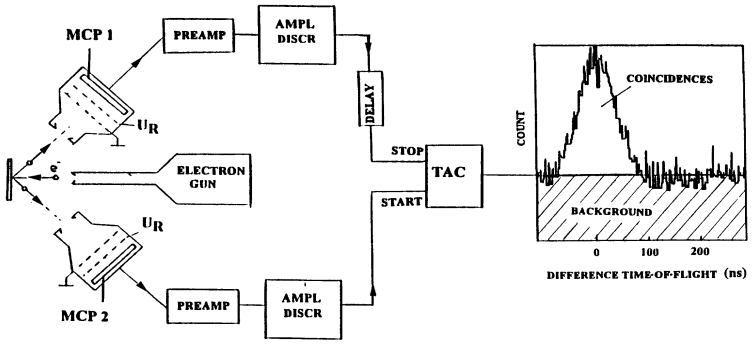

FIG. 1. Schematic view of the two-electron coincidence experiment in the reflection geometry. MCP is the microchannel plate and U_R is the retarding potential applied to the grids. The right-hand panel is a time-of-flight difference spectrum, showing difference in arrival of the "start" and "stop" electrons. Zero point is shifted by a delay in the "stop" channel.

from the lattice of adsorbed carbon and $(\frac{1}{2}0)$ from the lattice of adsorbed oxygen. A typical value of the (01) beam intensity relative to the background was 5–10, while $(\frac{1}{2}\frac{1}{2})$ and $(\frac{1}{2}0)$ spots were not observed after high-temperature flashes. The W(100) sample had been oriented in such a way that the (01) diffraction beam was in the detector plane. The residual gas pressure during the measurements did not exceed the 10^{-11}-mbar range. During the measurements the sample was periodically heated up to 70–1000 °C to remove adsorbed gases from the sample surface. The magnetic field of the earth had been reduced by about 100 times using Helmholtz coils and a μ-metal screen inside the vacuum chamber. The primary-electron beam current I_0 was kept at such a level that the count rate of each of the detectors was in the range of $5\times10^3-10^4$ s^{-1}. This corresponded to a primary current below 10^{-13} A.

The technique of measuring true coincidence events was briefly described in Ref. 6. One of the electrons of a correlated pair entering one of the detectors creates a start pulse for a time-to-amplitude converter (TAC). The second electron of the pair entering the other detector produces a stop pulse for the TAC. At the output of the TAC appears a signal which is proportional to the difference between the times of flight from the sample to the detector for the two electrons belonging to the pair. The coincidence-event number as a function of the electron time-of-flight difference is stored in a PC memory. A typical time-of-flight distribution of the coincidence events is shown in Fig. 1 (right-hand panel). The distribution maximum corresponds to equal times of flight of the two correlated electrons. The position of the maximum in Fig. 1 is shifted relative to the origin of coordinates by a certain value corresponding to the time delay introduced into the "stop" channel of the registration circuit. The full width at half maximum of the time-of-flight distribution for $E_p=16$ eV is about 90 ns. Uncorrelated start-stop events may have any time interval between start and stop (because in this case start and stop electrons are produced by different primary electrons) and thus appear as a "white noise" background in Fig. 1.

EXPERIMENTAL RESULTS

The number of coincidence events as a function of the primary-electron energy (relative to the Fermi level) is shown in Fig. 2. The coincidence-event number was normalized to 10^6 start pulses. The detectors are placed at the angle of $\pm40°$ to the sample surface normal. The primary-electron direction was normal to the surface. The experimental errors shown in Fig. 2 correspond to one statistical deviation. The solid and dashed curves in Fig. 2 represent the results of a model calculation for the

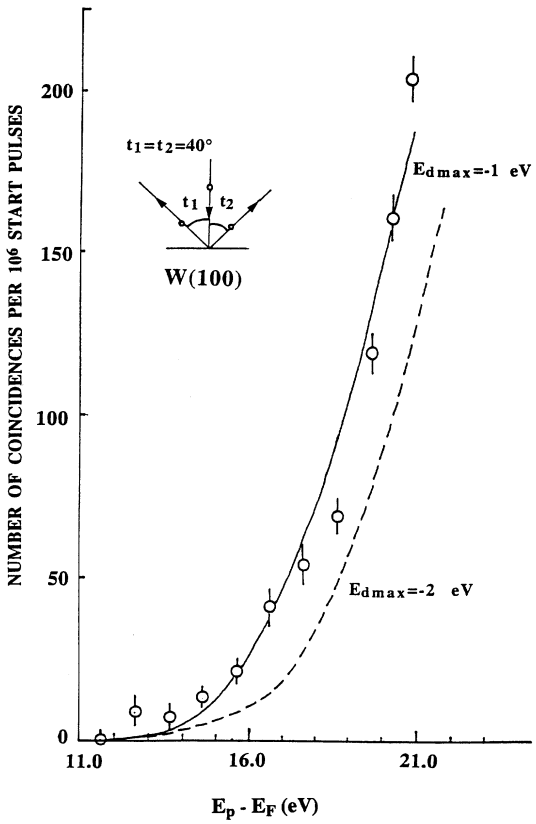

FIG. 2. CE number as a function of the incident electron energy. Dots with bars: experimental data for a symmetric arrangement, angle of incidence $\Theta=0°$, detection angles $t_1=40°$, $t_2=-40°$. Solid and dashed lines: calculated curves. Parameters of calculation: potential well bottom $E_b=-10$ eV, potential well top $E_t=4.6$ eV, energy position of the top of occupied d band $E_{d\,\max}=-1$ eV (solid line), $E_{d\,\max}=-2$ eV (dashed line).

TCE relative number as a function of the primary-electron energy and will be discussed later. The most significant difference between the distribution in Fig. 2 and that shown in Ref. 6 is the presence of a low-energy "tail" in the region below 18 eV. The coincidence-event appearance threshold in Ref. 6 had been determined as $E_{th}=18$ eV using linear extrapolation of the energy dependence in the low-energy region. Let us note that, if only the energy conservation requirement were taken into account, ignoring the momentum conservation requirement, the energy threshold for the emission of two electrons into vacuum would be equal to twice the work function value, i.e., it would be $E_{th}=9.2$ eV. The distribution shown in Fig. 2 demonstrates that the observed threshold value is shifted down to about $E_{th}=12$ eV. It can be seen from Fig. 2 that the coincidence-event number below ~ 12 eV is zero within one statistical deviation. However, we have no independent experimental result to confirm that this threshold value corresponds to a "physical" threshold rather than to the sensitivity of the measurement. The normalization of the CE number to 10^6 start pulses used in Fig. 2 means that the CE number is normalized to 10^6 scattered electrons entering the detector aperture. The ratio of the number of elastically scattered electrons to that of the inelastically scattered changes with the primary-electron energy. The elastic-reflection component of the scattered electron current was measured with a retarding potential applied to the second grid of the detector. It was found that the fraction of the elastically reflected electrons decreases as the primary-electron energy increases (from about 40% at $E_p=12$ eV to about 27% at $E_p=20$ eV). This decrease is insignificant compared with a sharp increase of the CE number. This comparison shows that the normalization of the CE number to the total number of electrons scattered in the detector direction or to the number of elastically scattered ones cannot make any significant difference in the energy position of the CE detection threshold.

An important feature of single scattering of a primary electron on a valence electron is the energy distribution between the two electrons of the resulting pair. The total energy of electrons of the pair is equal to the primary-electron energy minus the valence-electron binding energy relative to the Fermi level. Figure 3 presents schematically the range of possible values of the energy (E_1 and E_2) of electrons belonging to the pair created as a primary electron with the energy E_p is scattered on a valence electron at the Fermi level or near it (i.e., its binding energy being close to zero). In this case, if the primary-electron energy is higher than the CE appearance threshold, the interval of possible energy values of one of the electrons of the pair is from $E_1=e\phi$ to $E_1=E_p-e\phi$, the energy of the other being $E_2=E_p-E_1$. In Fig. 3 this requirement is fulfilled in the narrow shaded area, the width of this area being proportional to the energy region of valence electrons taking part in the scattering.

If retarding potentials U_{R1} and U_{R2} are applied to the detector grids then only that fraction of the correlated pairs can be detected for which the following inequalities

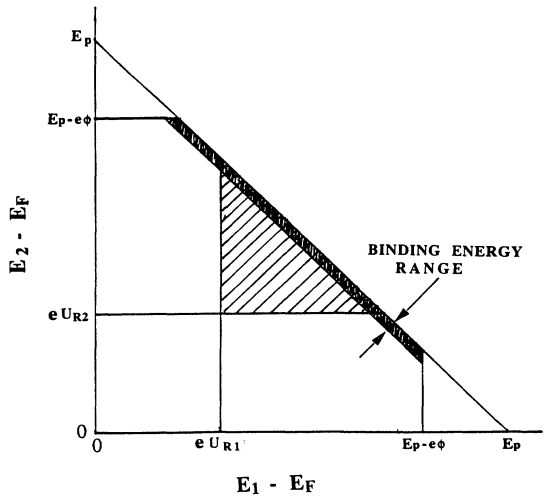

FIG. 3. Diagram showing the range of possible values of the energy E_1 and E_2 of electrons belonging to the pair created by a primary electron with the energy E_p. The narrow shaded area corresponds to excitation of valence electrons from the levels in the Fermi-level vicinity. The lightly shaded area defines possible values of correlated electron energies, when retarding potentials U_{R1} and U_{R2} are applied to the detector grids.

are valid: $E_1-e\phi>eU_{R1}$ and $E_2-e\phi>eU_{R2}$. It means that in Fig. 3 energy values of the electrons of the correlated pairs occur in the lightly shaded area limited by three straight lines: $E_1=eU_{R1}+e\phi$, $E_2=eU_{R2}+e\phi$, and $E_1+E_2=E_p$. In a special case when the valence-electron binding energy is zero, the hypotenuse of this right-angled triangle corresponds to the range of energy of the correlated electrons.

Figure 4 presents the CE number as a function of the retarding potential applied to the second grids of both detectors at the primary electron energy $E_p=20.6$ eV and in the above-described experimental geometry (both detectors are at $\pm 45°$ relative to the normal to the sample surface). The relative CE numbers plotted on the experimental curve are normalized to the storage time at a constant primary-electron current, the error bars corresponding to one statistical deviation. The values of the retarding potential $U_R=U_{R1}=U_{R2}$ are plotted on the abscissa axis. The solid line represents model calculations and will be discussed later. As the retarding potential increases from zero, the CE number changes insignificantly in the region $U_R<2$ eV, which shows that the correlated pairs comprise a relatively small amount of electrons whose kinetic energy in the vacuum is less than 2 eV. As the total energy of the electrons of a pair is constant and cannot exceed the primary-electron energy, it follows that the correlated pairs also contain relatively few high-energy electrons. From the total-energy conservation requirement we expect that at the retarding potential values $U_R>(E_p/2-e\phi)/e$ the number of detected CE's should be zero as one of the correlated electrons always has the energy $E<E_p/2$. For the primary-electron energy $E_p=20.6$ eV and with the work function of

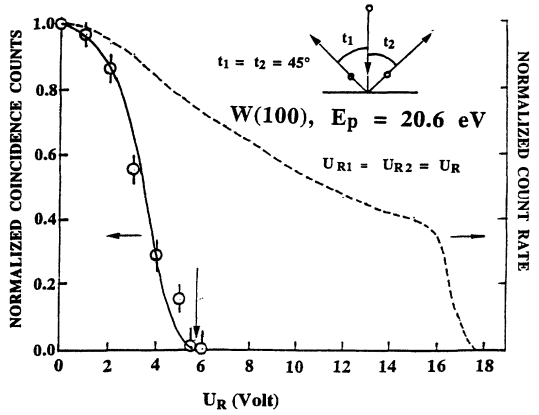

FIG. 4. Number of true coincidence events as a function of retarding potential applied to detector grids. Angle of incidence $\Theta=0°$, detection angles $t_1=45°$, $t_2=-45°$, retarding potentials $U_{R1}=U_{R2}=U_R$. The arrow indicates the energy-conservation-law limit ($U_R=5.7$ V). Parameters of calculation are the same as in Fig. 2. The right-hand scale is the secondary-electron rate (dashed curve).

tungsten ~ 4.6 eV taken into account, the upper limit of the curve in Fig. 4 should be observed at $U_R=5.7$ V (as shown by an arrow in Fig. 4), which is in quite good agreement with the experimental data.

We show further in Fig. 4 that the CE number dependence on the retarding potential is quite different from the usual dependence of the count rate of a single detector versus retarding potential applied to the grid of this detector (see dashed curve). In the latter case, for each of the registration channels the retarding potential curve extends from zero to $U_R=E_p/e$ as no limitations are imposed on the energy of the electron detected in the other channel.

Figures 5(a) and 5(b) show angular distributions of the

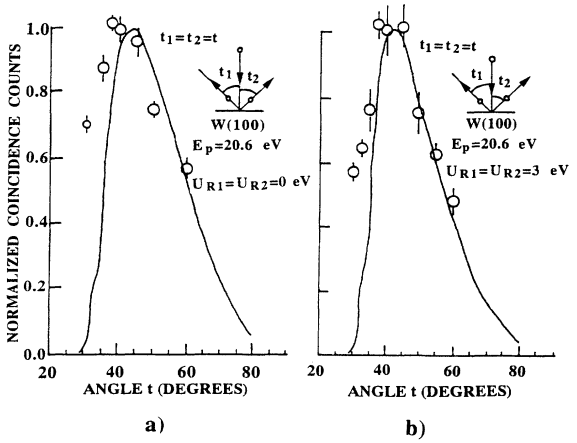

FIG. 5. Angular distribution of correlated electron pairs. Angle of incidence $\Theta=0°$, detection angles $t_1=-t_2$, $|t_i|=t$. Open dots with bars: experimental data for $E_p=20.6$ eV, (a) $U_R=0$, (b) $U_R=-3$ V. Solid line: model calculation. Parameters of calculation are the same as in Fig. 2.

CE number at the primary-electron energy $E_p=20.6$ eV and normal incidence. The angles of the detectors were changed simultaneously so that $t=t_1=t_2$. The CE number is normalized to the acquisition time for every experimental point at the same (fixed) primary-electron current, i.e., in fact, to a quantity proportional to the primary-electron number. The angular distribution of the CE number exhibits a maximum at the detection angles $t_1=-t_2=(30-40)°$. The curve in Fig. 5(a) was obtained at zero retarding potential on the detector grids, while the curve in Fig. 5(b) was measured at the retarding potential $U_R=3$ V applied to the grids of both detectors. Both the energy position of the maximum and its full width at half maximum changes insignificantly with the elimination of the lowest-energy electrons (by applying the retarding potential).

It can be seen from Figs. 5(a) and 5(b) that the most probable scattering angle in vacuum is 80°–86°. The most probable scattering angle in a previous experiment at the primary-electron energy of 30–45 eV and for a different scattering geometry was found to be 60°–75°.[7]

THEORETICAL MODEL OF SINGLE SCATTERING

We consider a simple kinematic model of scattering of a primary electron with the energy E_p and momentum $\mathbf{k}_p$ (the atomic system of units is used for simplicity where $e=m=1$ and angles are in radians) on a valence electron with the energy E_v and momentum $\mathbf{k}_v$ (Fig. 6).

The basic assumptions of the model are as follows.

(1) The valence electron has an equiprobable direction of the momentum $\mathbf{k}_v$ in space, i.e., is uniformly distributed over a sphere of radius k_v in momentum space.

(2) The primary electron, after elastic scattering, is also uniformly distributed over a sphere of radius k_p, i.e., its velocity direction in space is isotropic. The latter assumption stems from the necessity for the primary electron to be elastically scattered into the back hemisphere before the electron-electron scattering event itself may occur. This point had been discussed in Ref. 6 and experimentally corroborated in Ref. 7.

(3) We assume that the cross section of the scattering event is independent of energy in the entire region of interest. We calculate the probability of detection of correlated electrons from purely kinematic considerations. This means that the probability for an electron to be scattered in a certain solid angle is equal to the ratio of this solid angle to the full solid angle of scattering.

The aim of our calculations is to evaluate the probability for the two electrons to enter simultaneously into the solid angles of detectors $d\Omega_1$ and $d\Omega_2$ in vacuum, or into corresponding solid angles and in the solid. We consider further the scattering event inside the solid using transformation relations for the differential solid angles when an electron crosses the solid-vacuum interface. Besides, we take into account that not all of the valence and primary electrons uniformly distributed in k space can take part in scattering events, but only those whose $\mathbf{k}$ vectors satisfy certain kinematical requirements of scattering. The selection rules for the $\mathbf{k}$ vectors result from the ener-

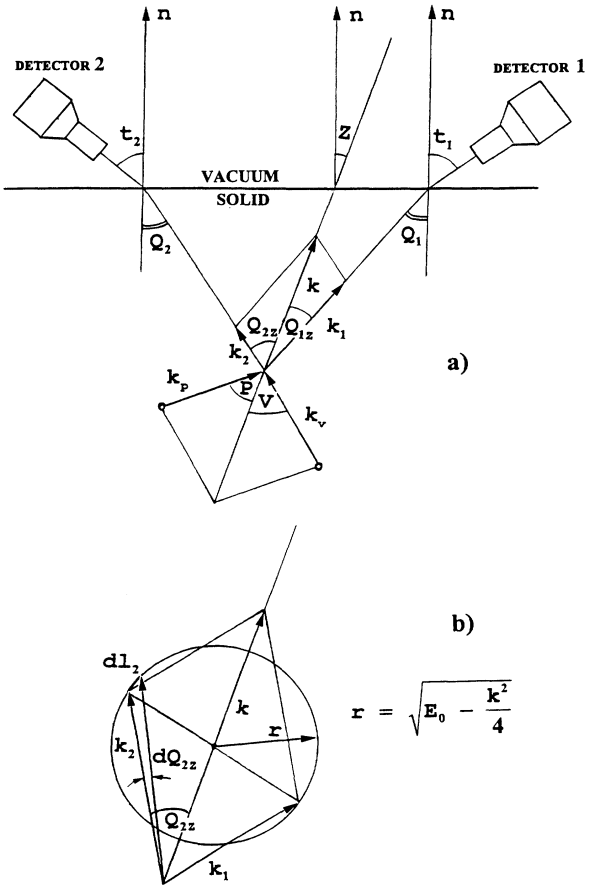

FIG. 6. Kinematical scheme of single-step scattering of the primary electron on the valence one. (a) Kinematical diagram of primary and valence electron scattering and escaping from the solid. (b) Energy and momentum conservation laws determine that momenta of two scattered electrons $\mathbf{k}_1$ and $\mathbf{k}_2$ are ending at the circle with the radius r. $\mathbf{k}_p$ and $\mathbf{k}_v$ are the primary-electron momentum and the valence-electron momentum before scattering, respectively, $\mathbf{k}$ is the total momentum of the two-electron system, $\mathbf{k}_1$ and $\mathbf{k}_2$ are the momenta of two scattered electrons, and $\mathbf{n}$ is normal to the sample surface.

gy and momentum conservation laws and the requirement that after the scattering event the electrons of the pair should travel within the solid angles defined by the detectors. So the probability for the valence electron to take part in scattering and be detected is equal to the ratio of the corresponding volume in k space to the full volume of valence-electron states. For the primary electron the probability of scattering in a certain solid angle is equal to the ratio of the corresponding area on a sphere of k_p radius in k space to the whole surface of the sphere.

A. Detection probability for the electron pair

For simplicity, we discuss below a special case when both scattered electrons with the energy E_1 and E_2 and momentum $\mathbf{k}_1$ and $\mathbf{k}_2$ travel in the same plane passing through the normal to the sample surface. In vacuum their momenta are $\mathbf{k}_1'$ and $\mathbf{k}_2'$, respectively. Their velocities are directed at the angles t_1 and t_2 to the normal in vacuum, or Q_1 and Q_2 in the solid. It is convenient to consider scattering of the electrons relative to the direction of the total momentum $\mathbf{k}$ of the two-electron system. In Fig. 6(a) the total momentum is directed at the angle Z to the surface normal. In this case the scattering has complete azimuthal symmetry relative to the Z' axis, which is chosen to coincide with the total-momentum $\mathbf{k}$ direction. Now we can go to a description of the scattering in one plane. From now on any momentum is considered as a scalar and any direction is given by a corresponding angle.

Going back to the scheme in Fig. 6(a), we consider scattering of a primary electron traveling after an elastic scattering event into the back hemisphere at the angle P to the direction of the total momentum of the system consisting of the primary electron and a valence electron. The valence electron travels at the angle V to the total momentum direction. After the electron-electron scattering event, a pair of electrons appears, which travel, respectively, at angles Q_{1Z} and Q_{2Z} to the total momentum direction and at angles Q_1 and Q_2 to the normal to the surface. Refraction of the electron trajectories at the interface changes the velocity directions and in vacuum the scattered electrons travel at angles t_1 and t_2 to the normal in the directions of the detectors.

The number of electron pairs created by one primary electron may be written as

$$\frac{d^6I}{dE\,dE_0 d\Omega_1 d\Omega_2} = N_v W W_v W_p \ , \tag{1}$$

here $d\Omega_1$ and $d\Omega_2$ are acceptance apertures of hypothetical detectors inside the solid, E is the energy of one of the electrons of the pair, E_0 is the total energy of the pair, N_v is the number of valence electrons, W is the probability for the electrons of the pair to occur (and to be detected) in the solid angles determined by the detectors, W_v is the probability for a valence electron to participate in a scattering event, the electrons being scattered into the solid angles $d\Omega_1$ and $d\Omega_2$ and in the differential energy intervals, and W_p is the probability for the primary electron to participate in a scattering event, the electrons being scattered into the solid angles $d\Omega_1$ and $d\Omega_2$ and in the differential energy intervals dE. W_v and W_p depend on polar angles Q_{1Z} and Q_{2Z} and they do not depend on azimuth angles because of the azimuthal symmetry of scattering relative to the Z' axis (which is chosen to coincide with the total momentum of the correlated pair). To calculate the number of detected correlated pairs of electrons we have to integrate expression (1) over solid angles of detectors $\Delta\Omega_1$ and $\Delta\Omega_2$ and over the full energy range of detected electrons ΔE and ΔE_0 (where ΔE is the energy range of detected electrons and ΔE_0 is the energy range of the total energy of the pair). The last value depends on the valence bandwidth because there is only one reason for creation of the pairs with different total energy E_0: namely, the scattering of primary electrons on valence electrons with differing binding energies.

B. Transformation of solid angles

Using the requirement of conservation of the tangential momentum component, it is easy to obtain expressions describing the solid-angle transformation when electrons pass from the solid to vacuum. It allows us to go to the description of the scattering events inside the solid. From the conservation of the tangential momentum component at the interface it follows that

$$Q_i = \arcsin\left[\left(\frac{E_i-E_t}{E_i-E_b}\right)^{1/2}\sin t_i\right] \quad \text{where } i=1,2\ . \tag{2}$$

The direction of the total momentum of the system inside the solid can be obtained from the ratio of the total-momentum $\mathbf{k}$ components normal and tangential to the surface, respectively.

$$Z = \arctan\left[\frac{k_1\sin Q_1+k_2\sin Q_2}{k_1\cos Q_1+k_2\cos Q_2}\right]\ . \tag{3}$$

The expression for the polar-angle transformation as we go from the vacuum to the solid is obtained by differentiating (2):

$$dQ_i=\left[\frac{(E_i-E_t)}{(E_i-E_b)}\right]^{1/2}\frac{\cos t_i}{\cos Q_i}dt \quad \text{where } i=1,2\ , \tag{4}$$

where dt is a differential of the detector polar angle, and E_t and E_b are the top and the bottom of the potential barrier on the solid-vacuum interface (see Fig. 7) (this will be discussed later).

An opening angle dt of a solid angle of the detector in the plane perpendicular to the polar plane is transformed into an azimuth angle in the plane normal to the total-momentum direction in the following way:

$$dU_{iZ}=\frac{k_i dt}{k_i\sin Q_{iZ}} \quad \text{where } i=1,2\ . \tag{5}$$

We chose the differentials of the components of detector solid angles both in the polar plane and in the perpendicular direction to be equal to dt (the detector apertures are circular).

C. Planar scattering

Now let us consider the scattering event itself resulting in scattering of one of the electrons into the angle dQ_1 and of the other one into the angle dQ_2. The total momentum of the two electrons and their total energy are conserved in the scattering event:

$$\begin{aligned} &E_0=E_p+E_v=E_1+E_2\ ,\\ &k_p\cos P+k_v\cos V=k_1\cos Q_{1Z}+k_2\cos Q_{2Z}=k\ ,\\ &k_p\sin P+k_v\sin V=k_1\sin Q_{1Z}+k_2\sin Q_{2Z}=0\ , \end{aligned} \tag{6}$$

where $Q_{1Z}=Q_1-Z$ and $Q_{2Z}=Q_2-Z$. For fixed values of E_0 and k describing the state of the two-particle system a range of possible values of E_1, Q_{1Z} and E_2, Q_{2Z} can be found. Solving Eqs. (6), it is easy to show that the end points of the vectors $\mathbf{k}_1$ and $\mathbf{k}_2$ lie on a circle of radius $r=\sqrt{(E_0-k^2/4)}$ with the center in the middle of the vector $\mathbf{k}$ [see Fig. 6(b)].

The equations describing the circle are

$$k_i=\begin{cases}\dfrac{k\cos Q_{iZ}}{2}+\frac{1}{2}(k^2\cos^2 Q_{iZ}+4E-2k^2)^{1/2} & \text{if } k_i>\frac{1}{2}k\cos Q_{iZ}\\ \dfrac{k\cos Q_{iZ}}{2}-\frac{1}{2}(k^2\cos^2 Q_{iZ}+4E-2k^2)^{1/2} & \text{if } k_i<\frac{1}{2}k\cos Q_i Z\ ,\end{cases} \tag{7}$$

where $i=1,2$. The endpoints of the vectors $\mathbf{k}_1$ and $\mathbf{k}_2$ are at the opposite ends of a diameter of the circle. Thus the final state of the system in the scattering plane is determined by only one independent parameter: either by the energy of one of the scattered electrons or by the direction of one of them.

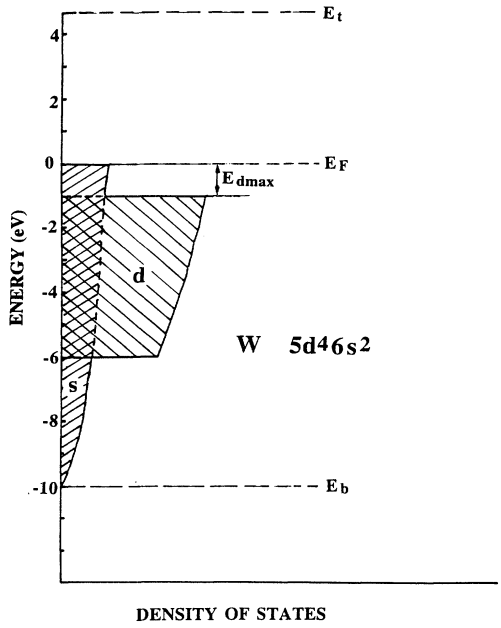

FIG. 7. Density of state of the valence band of tungsten in the two-parabolic-band approximation. The top and the bottom of the potential barrier relative to the Fermi level are $E_t=4.5$ eV and $E_b=-10$ eV.

D. Differential scattering probability

Let us determine the detection probability for a pair after scattering of one of the electrons with the momentum $\mathbf{k}_1$ into a polar angle dQ_1 and of the other electron with the momentum $\mathbf{k}_2$ into a polar angle dQ_2. This probability is determined by the ratio of the arc dl cut by a polar component of the solid angle on a circle of radius r to the total length of the circle. The length of this arc can be written as follows:

$$dl_i = \left[k_i^2 + \left[\frac{dk_i}{dQ_i} \right]^2 \right]^{1/2} dQ_i \quad \text{where } i=1,2 \ . \tag{8}$$

The probability for each of the electrons of the pair to be detected within the angle dU_{1Z} (or dU_{2Z}) is proportional to the value of this angle, because of the azimuthal symmetry of scattering relative to the direction of the total momentum. As we consider only scattering in the plane passing through the normal to the surface, the azimuthal angles of the vectors $\mathbf{k}_1$ and $\mathbf{k}_2$ ought to differ by π radian.

The probability for the pair to be detected is equal to the smallest of the two detection probabilities for the electrons of the pair; therefore the probability of scattering into solid angles d_1 and d_2 can be written as

$$W = \frac{dl_{\min}}{2\pi(E_0 - k^2/4)^{1/2}} \frac{dU_{Z\min}}{2\pi} \ , \tag{9}$$

where $dl_{\min} = \min(dl_1, dl_2)$ and $dU_{Z\min} = \min(dU_{1Z}, dU_{2Z})$. Expression (9) describes the probability of scattering of a primary+valence electron pair characterized by the total energy E_0 and total momentum $\mathbf{k}$, resulting in the electrons going out at the angles Q_{1Z} and Q_{2Z} relative to the total-momentum direction or, which is the same, at the angles t_1 and t_2 to the normal in vacuum, into solid angles with the linear opening dt.

The energy value E_1 and E_2 of the electrons of the pair with fixed total energy and total momentum are unambiguously related to the scattering angles. The energy increment dE_1 for the electron with the momentum $\mathbf{k}_1$ and dE_2 for the electron with the momentum $\mathbf{k}_2$ can be defined as

$$dE_1 = k_1 \left[\frac{dk_1}{dQ_1} \right] dQ_1, \quad dE_2 = k_2 \left[\frac{dk_2}{dQ_2} \right] dQ_2 \ ,$$
$$dE = \min(dE_1, dE_2) \ . \tag{10}$$

If we integrated (1) over the acceptance angles of the detectors, the fact that the smaller of the two acceptance angles restricts the final probability would be taken into account automatically.

E. Probability for valence and primary electrons to take part in the pair creation

Now we must determine the probability of valence electrons being involved in scattering, W_v. Correlated pairs with various total momenta may enter the apertures of the detectors. Thus, if the direction of one of the electrons is fixed (Q_1), a change of the second electron scattering angle in the interval $(Q_2, Q_2 + dQ_2)$ leads to a change of the total momentum k, and accordingly to a situation when both the primary and the valence electron involved in the scattering have different velocity directions. The angles Q_1 and Q_2 in this case must be considered as independent parameters, varying in the limits set by the detector apertures.

Solving Eqs. (6) it is possible to obtain an unambiguous relation between the momentum directions of the primary, valence, and scattered electrons:

$$V = \arccos \frac{k^2 - k_p^2 + k_v^2}{2k_v k} \ ,$$
$$k = k_1 \cos Q_{1Z} + k_2 \cos Q_{2Z} \ , \tag{11}$$
$$P = \arcsin \left[-\frac{k_v \sin V}{k_p} \right] \ ,$$

where V and P are the angles of the valence- and primary-electron momenta to the total momentum before scattering [see Fig. 6(a)].

Then the angle increments dV and dP are given by the following expressions:

$$dV = \frac{\partial V}{\partial Q_1} dQ_1 + \frac{\partial V}{\partial Q_2} dQ_2 \ ,$$
$$dP = \frac{dP}{dV} dV \ , \tag{12}$$

where $\partial V/\partial Q_1$ and $\partial V/\partial Q_2$ are partial derivatives of expression (11).

W_v is equal to the ratio of the volume in k space in the valence state region participating in the scattering to the total volume of valence states $\mathcal{V}_v$. Taking into account (11) and (12) we find

$$W_v = |2\pi \, dV \sin V k_v \, dE| \frac{1}{\mathcal{V}_v} \ . \tag{13}$$

W_p is equal to the ratio of the fraction of the equipotential surface of the primary electrons fulfilling the scattering requirements relative to the total surface S_p of the sphere of the radius k_p:

$$W_p = |2\pi \, dP \sin P k_p^2| \frac{1}{S_p} \ . \tag{14}$$

To obtain the coincidence rate per one isotropically elastically scattered primary electron, one should integrate (1) over all possible energies of the electron pair and over the detector apertures. The limits of integration over the energy of the electrons of the pair depend on the detection conditions, the work function of the surface, and on the retarding potential applied to the detectors grids. It is convenient to choose the integration step taking into account the electron energy increment in a unit angle increment [Eq. (10)]. In fact, this is the integration over the interval of possible values of the total momentum of the system, and the integration over the total energy of the pair is the integration over the valence band.

F. Model of the solid

Characteristics of the solid enter the calculation through the parameters of the surface potential barrier and the character of valence states. We assume that the surface potential barrier is a step function and denote the energy positions of its bottom and top relative to the Fermi level as E_b and E_t, respectively. Thus, $E_t - E_F$ is equal to the work function.

All the electrons involved in the scattering process are assumed to obey the quadratic dispersion law. To take into account, if only roughly, the complicated structure of the tungsten valence band with its $6s^2 5d^4$ configuration, we have used the two-parabolic-band approximation shown in Fig. 7.

The kinetic energy of all the electrons inside the solid is referred to the bottom of the potential barrier and of those in vacuum to the top of the barrier. The s band is entirely occupied from the bottom of the potential barrier to the Fermi level. The d-band electrons occupy the states from $E_{d\,\min}$ and $E_{d\,\max}$. Normalization in Eq. (13) is made to the volume ($\mathcal{V}_v$) of occupied parts of the s and d bands.

In our recent paper[7] we used a slightly different model of the valence-band structure of tungsten to calculate the angular dependence of the correlated pairs and the same kinematical model of scattering. The main points by which the previous model of the valence-band structure differs from the present one are (a) the kinetic energy of s-band electrons is related to the bottom of the s band and the kinetic energy of the d-band electrons to the bottom of the d band (in the present case the kinetic energy of electrons in the solid is related to the bottom of the potential barrier which coincides with the bottom of the s band), and (b) previously, we used the effective mass of valence electrons as a parameter to fit the experimental data, while in the present case the mass of valence electrons is assumed to be equal to the free-electron mass. Thus it is possible now to use only two independent parameters to fit the experimental results for tungsten. The question on the reference level for the kinetic energy of valence electrons is still open. In the present case we found a fair agreement of experimental and calculated curves under the assumption that the zero kinetic-energy level is approximately equal to the zero of the muffin-tin potential.

DISCUSSION OF THE RESULTS

A comparison of the model calculations and the experimental results allows a better understanding of the main features of electron scattering and emission of correlated pairs.

We assumed the tungsten work function to be $e\phi = 4.6$ eV. As fitting parameters we used the potential barrier depth E_b and the energy position of the top of the occupied d-band valence states $E_{d\,\max}$. A satisfactory agreement between calculated and experimental curves can be obtained if we choose $E_b = -10$ eV and $E_{d\,\max} = -1$ eV. These values agree with those obtained in the tungsten band-structure calculations,[8] where the muffin-tin-potential value was 11.8 eV and the d-band top lay at approximately -1 to -1.5 eV. We do not consider it worthwhile to try to achieve a better fit, because, first, the description of the tungsten valence band by a combination of two parabolic bands is a rather crude approximation, and, secondly, the kinematic scattering model we used is also a very simple approximation.

Now, what are the main features of coincidence spectroscopy in back-reflection geometry?

In Ref. 1 we considered a simple case of a primary electron traveling from the inside of the solid to its surface and scattering on a valence electron, which was assumed to be at rest. It was shown that the minimum primary-electron energy for emission of both electrons into vacuum equals four times the work function of the material (in this case both electrons are emitted tangentially to the surface). If we now take into account the valence-electron finite velocity and also the surface potential barrier depth, then we obtain a primary-electron threshold energy value of about $E_{\rm th} = 12$ eV relative to the Fermi level for the case of electrons detected at angles $t_i = \pm 40°$ (see the full curve in Fig. 2). The calculated values were multiplied by a scaling factor to make the ordinates of the experimental and calculated curves match at the point $E_p = 15$ eV, because we calculated only the relative number of the TCE's versus primary-electron energy and did not calculate the scattering matrix element. The calculated curve was normalized to one elastically scattered electron, while the experimental one was normalized to the total number of scattered electrons. As the ratio of the number of the elastically scattered electrons to the total number of scattered electrons depends only slightly on the primary-electron energy, the agreement between the two curves in Fig. 2 may be considered satisfactory. Near the CE appearance threshold the primary-electron scattering occurs on the fastest valence electrons in the vicinity of the Fermi level. As the energy E_p increases, the deeper-lying valence bands become involved, but the probing of the valence band is not proportional to the excess energy over the threshold. For example, valence electrons with the energy -1 eV begin to be involved in the scattering at $E_p = 16$ eV. In Fig. 2 the initial increase in the $E_p = 12$–16-eV region corresponds to scattering on s-band electrons. At energies higher than $E_p = 16$ eV scattering on d-band electrons begins to occur.

Figure 8 shows the number of coincidences as a function of the primary-electron energy for different work function values.[6] The increase of the work function and its decrease were achieved by oxygen and cesium adsorption, respectively. The curves calculated according to the present model are also shown in Fig. 8 for comparison.

The calculated dependence of the relative TCE number on the retarding potential (Fig. 4, full line) was obtained by changing the integration limits when expression (1) was integrated over energy in such a way that for each retarding potential value the requirement of the kinetic energy of scattered electrons in vacuum being higher than the retarding potential was fulfilled: $E_1 - E_t > eU_R$, $E_2 - E_t > eU_R$. Thus the calculated dependence was obtained for comparison with the experimental curve measured with the same retarding potential at the grids of

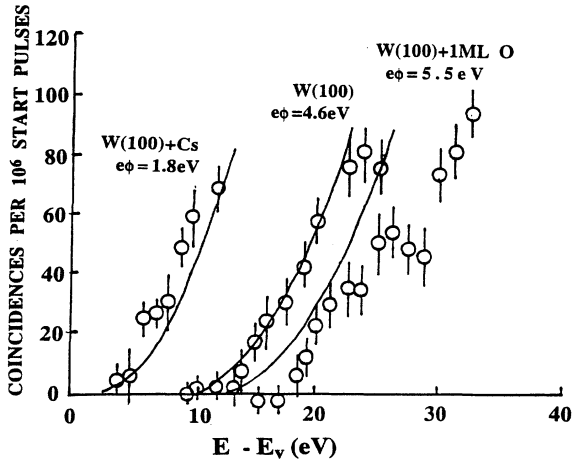

FIG. 8. CE number as a function of the incident electron energy for three different values of the work function of the W(100) crystal [for a clean crystal and with Cs or O adsorbed on its surface (Ref. 6)]. Solid lines present the results of calculation. Parameters of calculation are the same as in Fig. 2 with the exception of the work function values.

both detectors. The experimental dependence is normalized to a quantity proportional to the incident electron number, while the calculated one is normalized to one elastically scattered electron. But as the coefficient of elastic scattering has not changed during the experiment, the relative changes of the experimental and calculated curves can be compared.

As was mentioned in the discussion of the experimental dependence in Fig. 4, and the calculated dependence supports this, there is a relatively small number of pairs with a large difference in the energies of the electrons belonging to one pair. In other words, there is a relatively small number of pairs in which the energy of one of the electrons is less than approximately 2 eV. At a primary-electron energy of 20.6 eV the bulk of the pairs has an energy in the range of 8–13 eV. This, as well as the CE number energy dependence, is evidence in favor of the suggestion that the pair creation occurs mostly as the result of scattering of 20.6-eV primary electrons on valence electrons near the Fermi level. The total energy of the electrons of the pair in this case is the maximum possible.

In Fig. 5 measured angular dependencies of the relative CE number are compared with the calculated ones. The experimental data are normalized to a quantity proportional to the incident electron number, while the calculated curves are normalized to one elastically scattered electron. So there is no difficulty in comparison of the curves. Calculated and experimental curves are in satisfactory agreement. The calculations predict the lower angle limit of the angular TCE dependence at the scattering angle of about $\pm 30°$ relative to the surface normal, or of about 60° between scattered electrons in vacuum. This minimum possible angle of scattering corresponds to the maximum total momentum **k** for the electron pair, i.e., to the case when the primary electron and the valence electron at the Fermi level travel parallel to each other.

The experimental dependence in Fig. 5(b) obtained at 3 V retarding potential at the detector grids is in a better agreement with the calculated dependence than the one presented in Fig. 5(a) obtained at zero retarding potential. The cause for this is, probably, the presence in the latter case of pairs with lower total energy, as a result of inelastic scattering. The shift of the maximum of the angular distribution in the direction of smaller scattering angles in Fig. 5(a) is due to detection of pairs including one low-energy electron. These pairs are not detected when a retarding potential is applied. Unfortunately, because of the experimental geometry limitations we could not go below the scattering angle of $\pm 30°$. Taking into account that the analyzer apertures were 14°, it can be said that the calculated angular distributions reproduce the main features of the experimental angular distributions.

The role of multiple electron scattering in the correlated pair creation

It is obvious that any electron-electron scattering event creates a pair of electrons. Not all of these pairs can exit from the solid because of additional elastic and inelastic scattering. The additional elastic scattering of any of the electrons of the pair changes the momentum of the pair while the additional inelastic scattering event changes the energy (and momentum) of the pair. The probability to detect a pair of electrons was measured to be about 4.10^{-4} per one inelastically scattered electron detected by the "start" detector at 20 eV energy of primary electrons. We refer now the number of the pairs to one inelastically scattered electron because the elastically scattered electron cannot be considered as one of the electrons of the pair. Approximately one-half of detected electrons are inelastically scattered primary electrons at $E_p = 20$ eV. If we assume that the second electron of a pair (detected as a "stop" electron) is distributed isotropically, its probability to be detected is equal to the ratio of the detector solid angle to the full solid angle, or $0.07/4 = 5.5 \times 10^{-3}$. This should be an underestimation because the momentum conservation law does not allow electrons to be scattered in every direction, but even this value is higher than the measured one by an order of magnitude. It is clear from this estimation that at 20 eV primary-electron energy there is an effective channel that decreases the number of pairs to be detected. Since for electron energies in the range 10–20 eV the inelastic scattering rate is substantially higher than the elastic one, we expect inelastic scattering to be responsible for this loss.

As has been mentioned above, the true coincidence event is a detection of a pair of electrons created in a single scattering event and without undergoing any other scattering. In fact, we measure by coincidence spectroscopy both true coincidence events and secondary-electron coincidence events. The "cascade" creation of secondary electrons leads to appearance of secondary electrons with different energies. Some of them, whose energy is higher than the threshold energy, can create correlated electron pairs. Both elastic and inelastic scattering of any elec-

trons of the pair lead to a loss of the momentum or energy correlation between electrons of the pair. We eliminate easily the accidental coincidence background originating from the random character of an electron emission. The selection of the TCE's from SECE's originating from additional elastic and inelastic collisions is more difficult because all these scattered electrons are produced by the same primary electron and therefore they are time correlated.

Let us consider the role of SECE's at the energy of incident electrons close to the threshold energy of TCE appearance. In accordance with our kinematic model of scattering, the threshold of TCE's is determined by the energy and momentum conservation laws. If correlated electrons are undergoing additional scattering the momentum conservation law for incident and correlated electrons vanishes, and the energy threshold of TCE's should be equal to twice the work function. We see from the experimental results that there are not any coincidence events, in the limits of experimental errors, in the energy region from the double work function value up to 12 eV, approximately. The latter value corresponds to the calculated threshold energy in the kinematic approximation. We can assume from this that the experimental energy threshold corresponds to the single scattering one of the true coincidence events and the role of SECE's becomes not so important in the energy region of the CE threshold.

CONCLUSIONS

In the present work we report new experimental data concerning coincidence spectroscopy of tungsten and discuss them and the data obtained earlier in the framework of a simple kinematic scattering model. The tungsten energy-band structure is described by a two-parabolic-band model which has only two fitting parameters: the depth of the potential well E_b and the energy position of the d-band top $E_{d\,\max}$. We found that with $E=-10$ eV and $E_{d\,\max}=-1$ eV relative to the Fermi level, a satisfactory agreement between the experimental and calculated curves can be achieved. This agreement is observed for the main features of various dependencies: for the energy threshold of the electron pair appearance, for the threshold energy shift accompanying variations of the surface work function, for the shape of the coincidence-rate dependence on the retarding potential, and for the shape of the angular distributions. The fact that dependencies so different in their character can be satisfactorily described by the same model argues in favor of the physical relevance of these parameters.

The kinematic scattering model is unable to describe the details of electron-electron interaction but it gives a certain basic knowledge about the characteristics of electron-electron scattering in a particular material and may serve as a basis for planning further experiments and data processing.

ACKNOWLEDGMENTS

Two of us (O.M.A. and S.N.S.) are grateful to the Max-Planck-Gesellschaft and to the Max-Planck-Institut für Mikrostrukturphysik for financial support and hospitality. This work was partially supported by the Science and Higher Education Committee of Russia.

*On leave of absence from Research Institute of Physics, St. Petersburg University, St. Petersburg, Russia.

[1]I. E. McCarthy and E. Weigold, Rep. Prog. Phys. **51**, 299 (1988).

[2]P. Hayes, J. F. Williams, and J. Flexman, Phys. Rev. B **43**, 1928 (1991).

[3]Chao Gao, A. L. Ritter, J. R. Dennison, and N. A. Holzwarth, Phys. Rev. B **37**, 3914 (1988).

[4]Jeff Drucker, M. R. Scheinfein, J. Lin, and J. K. Weiss, J. Appl. Phys. **74**, 7329 (1993).

[5]M. R. Scheinfein, Jeff Drucker, and J. K. Weiss, Phys. Rev. B **47**, 4068 (1993).

[6]J. Kirschner, O. M. Artamonov, and A. N. Terekhov, Phys. Rev. Lett. **69**, 1711 (1992).

[7]O. M. Artamonov, M. Bode, and J. Kirschner, Surf. Sci. **307-309**, 912 (1994).

[8]N. Egede Christensen and B. Feuerbacher, Phys. Rev. B **10**, 2349 (1974).